Facile chemical activation of graphite felt by KMnO4 acidic solution for vanadium redox flow batteries

Ali Hassan, Théodore Tzedakis

Facile chemical activation of graphite felt by $KMnO_4$ acidic solution for vanadium redox flow batteries

Ali Hassan*, Theodore Tzedakis*

Laboratoire de Génie Chimique, UMR CNRS 5503, Université de Toulouse, UT-III-Paul Sabatier, 118 Route de Narbonne, F-31062 Toulouse, France

Keywords:
Graphite felt chemical activation
Vanadium redox flow batteries
Charge–discharge cycles
GF surface free energy
Intrinsic heterogeneous electronic transfer constant

A B S T R A C T

The activation method is proposed to enhance the electroactivity of the graphite felt (GF), to be used as positive half-cell electrode for vanadium redox flow batteries (VRFBs). Two following activation approaches are used 1) functionalization of electrode surface by the chemical treatment with acidic solution of the $KMnO_4$ and 2) deposition of $KMnO_4$ derived particles on the surface of GF. The intrinsic heterogeneous electronic transfer constant (k°) of $V^{(V)}/V^{(IV)}$ system is enhanced by 2.6 and 6.1 times for the oxidation ($V^{(IV)} \rightarrow V^{(V)}$) and reduction ($V^{(V)} \rightarrow V^{(IV)}$) reactions, respectively. The performed electrolysis in the half-cell shows the improved reversibility of the electrode. The treated electrode is also evaluated on the stack level by using 100 cm^2 GF in each electrolytic section of the battery, by charge and discharge cycles. The results clearly indicate the lowering of anodic and cathodic overvoltage, i.e. the average charging voltage decreases from 1.86 V to 1.76 V, while the obtained voltage during discharge increases from the 0.59 V to 0.8 V. The proposed activation method is operationally simple; and activated electrode shows the promising performance as positive half-cell electrode in VRFBs.

1. Introduction

Renewable energy has been getting prime importance since few decades because of diminishing conventional power resources and environmental challenges. But the intermittent nature of these resources, limits their viability and raise the question of their sustainability on commercial scale. Effective energy storage systems are important to shear off the gap between the supply and demand; and to align it with the load requirements. Redox flow batteries (RFBs) can successfully overcome this practical limitation because of their underlying characteristics of detached energy and power density. There is the advantage of flow batteries over conventional lead-acid batteries, that the energy is stored in the electrolyte, outside of stack. So, the capacity of flow batteries depends on concentration and the volume of electrolyte. Due to this, the scale up of battery is easy; as it requires just to alter the volume of electrolyte, without changing the stack.

Different redox couples (Fe/Cr, V/Br, Zn/Ce, bromine/polysulphide) with wide potential gap, have been investigated for the flow batteries [1–5]. For large scale energy storage applications, the electrolyte stability for long time is very importance; but using different redox couple in catholyte and anolyte leads to the cross contamination of the electrolyte. In addition to that, it also causes the self-discharge of the flow cell. This problem can be minimized by employing the same metal ions in both compartment of the flow battery, such as in the case of all vanadium redox flow batteries (VRFBs) [6–9] The vanadium element exits in four different valencies "$V^{(II)}$, $V^{(III)}$, $V^{(IV)}$, $V^{(V)}$". The idea of using vanadium in both half cells of flow battery was first floated by the Prof. Skyllas Kazacos [10]. The primary redox reactions in the positive and negative half-cell are represented by the eq. (1) and (2), respectively. The standard overall cell voltage is 1.26 V.

$$\text{Positive electrode: } VO_2^+ + 2H^+ + e^- \rightleftharpoons VO^{2+} + H_2O \quad E^\circ(VO^{2+}/VO_2^+) = 1.00 VvsSHE; \tag{1}$$

$$\text{Negative electrode: } V^{3+} + e^- \rightleftharpoons V^{2+} \quad E^\circ(V^{2+}/V^{3+}) = -0.26 VvsSHE; \tag{2}$$

These redox reactions are taking place on electrodes; and hence, the power density of the flow cell depends on the active surface area of the electrodes and its electro-kinetic activity . So, the selection for the electrode material is critical in the optimization of the vanadium redox flow battery stack. It is also important, because the stack is contributing approximately 30% of the total cost of VRFBs [11]. Many carbon electrode materials have been investigated so far, to be used as electrode for the vanadium redox flow batteries i-e carbon paper, glassy carbon, graphene oxide, graphite fibers, graphite felt, carbon felt and multiwalled carbon nanotubes etc. [12–14]. The PAN based graphite felt with 3D fibrous structure, is potential candidate as electrode material for the VRFBs, because of its significant surface area [15]; in

* Corresponding authors.
E-mail address: hassan@chimie.ups-tlse.fr (A. Hassan).

https://doi.org/10.1016/j.apsusc.2020.146808

addition to that, it is very stable in acidic conditions. However, it shows very poor kinetic reversibility against vanadium redox flow couples [16].Different strategies are reported in literature to enhance the electrocatalytic activity of the graphite felt by electrochemical, chemical and thermal activation methods, but most often they are complicated, prolong and involved complicated experimental setups. The purpose of these methods is to increase the available surface area and fabricate different functional groups on surface. The increase in the active surface area helps the battery to achieve higher current operating currents; while the different functional groups of the oxygen and nitrogen act as catalyst, resulted into the lowering of the activation overpotential [17–26]. Different metals and their oxides (Pt, ZrO_2, Nb_2O_5, CeO_2, Pd, PbO_2, Au etc.) also facilitate to overcome the kinetic limitation of the carbon electrodes towards the vanadium redox flow couples[27–31]. But most often they are expensive; and their mechanical stability is also questionable in the flow conditions of acid electrolyte. Metal oxides also accelerate the secondary reactions of the O_2 and H_2 formation, which narrows down the operating voltage window of the battery[32–33]. The negative half-cell redox reaction is relatively faster and more reversible than positive half-cell reaction, as it involves one electron transfer step ($V^{2+} \rightleftharpoons V^{3+}$); while the positive half-cell reaction($VO_2^+ \rightleftharpoons VO^{2+}$) undertake one additional step of oxygen transfer [34–36]

Robert [37] discussed that the strong oxidizers like $KMnO_4$ can be used to activate the carbon-based electrode by thermal and electrochemical treatment for flow batteries. The patent content is very general and qualitative; moreover, the expected effects, at the least in the positive electrode of vanadium redox flow battery, were not indicated. In this study, two different approaches were investigated to activate the GF, to use as positive half-cell electrode in VRFBs. In first approach, the GF was heated at 140 °C for 2 h in 0.01 M $KMnO_4$ acidic solution, under non-reflux conditions. The method modified the surface chemistry and morphology of GF successfully, by fabricating the oxygenal groups on its surface and incorporate more roughness on it. The activated GF showed enhanced electro-kinetic activity, as positive half-cell electrode. In another method, the $KMnO_4$ derived particles were fabricated on the GF, but it did not show any catalytic activity towards positive half-cell redox reaction. It is important to note, that Wang et al. [38] fabricated the MnO_2 nanosheets array-decorated carbon paper by $KMnO_4$ and it showed improved electroactivity as negative half-cell electrode in VRFBs.

2. Experimental

2.1. Materials

All the chemicals were of analytical grade and not required further processing. Vanadium (IV) oxide sulfate hydrate $VOSO_4{\cdot}xH_2O$ and potassium permanganate $KMnO_4$ were provided by the VWR international, France. The nafion membrane (N-424) was purchased from the Ion power Inc. USA. The Sulphuric acid (95–97%) was purchased from the Sigma-Aldrich Co. France. Poly acrylonitrile (PAN) based graphite felt (GF) of 3 mm thickness, and platinum wire of 0.125 mm thickness (99.95%) were provided by Goodfellow Cambridge Ltd. France.

2.2. Electrode preparation

In this study, GF was activated by adopting two different approaches. First approach is concerned to change the surface chemistry and roughness of the GF, by heating it in the $KMnO_4$ acidic solution and named as class-1 for further reference. Second approach is concerned to fabricate residuals potassium permanganate particles on the surface of the GF, to analyze their effect against $VO^{2+}/VO_2{}^+$ reaction and described as Class −2 in further text. Both are discussed in detail, as following.

2.2.1. Class −1 approach

The purpose of this treatment is to functionalize the surface of the GF by harnessing the oxidizing power of acidic $KMnO_4$ solution. For this, the commercial GF was thoroughly rinsed with the distilled water and used as reference (untreated-GF). After, it was pretreated at 400 °C for 2 h in muffle furnace to had better solution interaction while chemical activation (400 °C –2h-GF). The annealed GF was heated at 140 °C for 2 h in 0.01 M $KMnO_4$ + 3 M H_2SO_4 solution, under non-reflux conditions ($KMnO_4$-140 °C-2 h-GF). Then the GF was washed with hot and cold distilled water several times to remove any kind of the acidic and $KMnO_4$ residues.

2.2.2. Class −2 approach

During this operation, two different GF samples were prepared to investigate the following two possibilities:

1) To fabricate the thermally cracked $KMnO_4$ particles on the GF and check their electroactivity against $VO^{2+}/VO_2{}^+$ redox system ($KMnO_4$-600 °C-N_2-GF).

2) To deposit the $KMnO_4$ particles (without chemical decomposition) on the GF and investigate their catalytic effect against the $VO^{2+}/VO_2{}^+$ redox system ($KMnO_4$-400 °C-air-GF).

First sample was prepared by dipping the GF in the beaker, containing 0.01 M $KMnO_4$ + 3 M H_2SO_4 solution , and then put this beaker in the oven at 80 °C until all the solution was evaporated. The obtained dry GF, covered with residual permanganate was heated at 600 °C in the nitrogenous environment for 90 min, to thermally decompose the $KMnO_4$ compounds and to have GF surface covered with cracked $KMnO_4$ particles ($KMnO_4$-600 °C-N_2-GF).

Second sample was prepared by adopting the similar procedure as above, except 1) the operating temperature was fixed for oven at 400 °C and 2) the presence of the air in the oven. The purpose of heating at 400 °C was to attach the residual permanganate on the GF surface. As the objective here, was not to thermally crack the $KMnO_4$, so the temperature chosen was lower (400 °C) than the previous one (600 °C). Both samples were washed thoroughly with the distilled water containing few drops of H_2SO_4

3. Electrode characterization

3.1. Electrocatalytic evaluations

The electrode electrocatalytic activity was evaluated at transient state by cyclic voltammetry (CV) in classical three electrode cell. The 1 cm^2 piece of the GF was precisely cut and subject to CV at the following experimental parameters; scan rate: 10 mV s^{-1}; in 0.05 M VO^{2+} + 2 M H_2SO_4 electrolyte; between the potential ratio of 0 V to 1.6 V in unstirred conditions. The platinum foil of 3 cm^2 and saturated calomel electrode (SCE) were used as counter and reference electrode, respectively.

Linear sweep voltammetry (LSV) curves were plotted with the precisely cut graphite felt of 1.5 × 1.5 cm^2 at the scan rate of 1 mV s^{-1} with stirring rate of 350 rpm. To study the kinetics of the of $V^{(IV)}$ to $V^{(V)}$ reaction on GF, the experiment was started from open circuit potential (OCP) towards the anodic direction, in solution of 0.5 M VO^{2+} + 3 M H_2SO_4. The anodic scan was stopped, when system approached 1.2 V.

The reverse scan was performed towards cathodic direction, in the electrolyte of 0.47 < $VO_{2(M)}^+$ < 0.49 + 3 M H_2SO_4, to evaluate the performance of GF for $V^{(V)}$ to $V^{(IV)}$ reaction. The $VO_2{}^+$ solution used for the reverse scan was obtained by the electrolysis of the 0.5 M VO^{2+} + 3 M H_2SO_4 solution, in the half cell.

3.2. Electrode surface characterization

The changes occurred in the surface chemistry of the GF were analyzed by the Fourier transform infrared spectroscopy (FTIR) on thermo Nicolet 6700 (Thermo Fisher Scientific, USA). The untreated

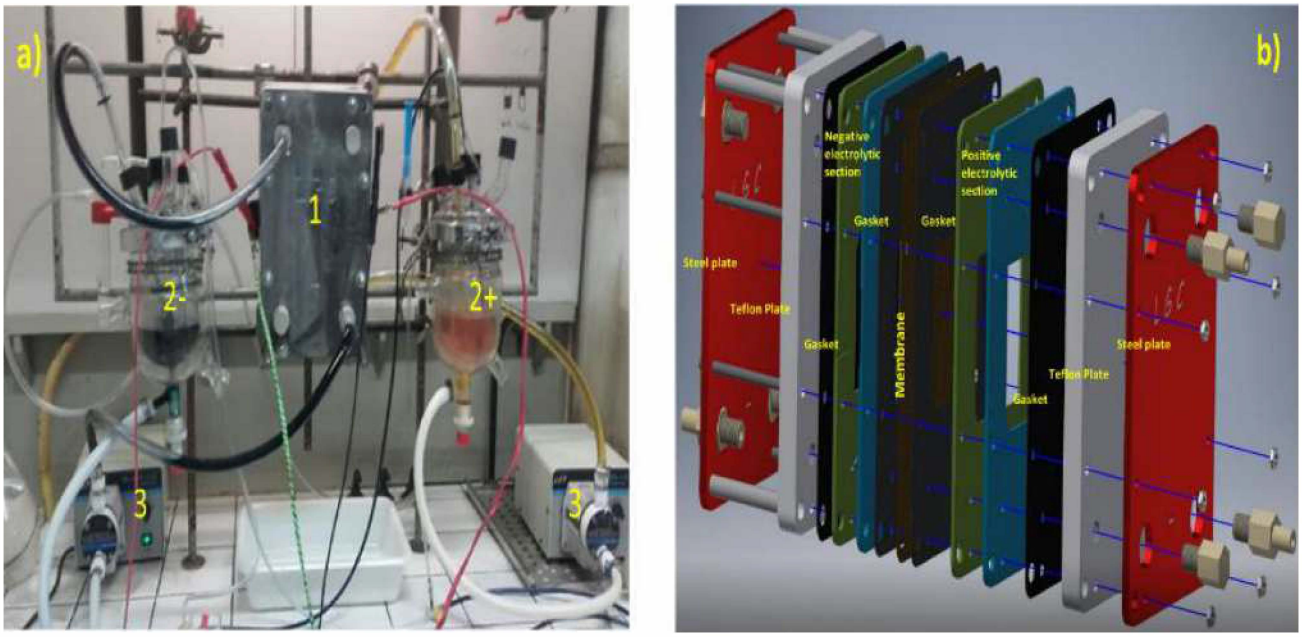

Fig. 1. a) The vanadium redox flow battery having electrochemical reactor with 10 cm × 10 cm electrodes (1), accompanied by posolyte (2 +) and negolyte storage tanks (2-) of 1 L capacity; with two pumps (3) for continuous flow of the electrolyte; b) The individual components of electrochemical reactor of VRFBs, comprising of steel plate, teflon plate, gaskets, membrane, positive and negative half-cell electrolytic sections.

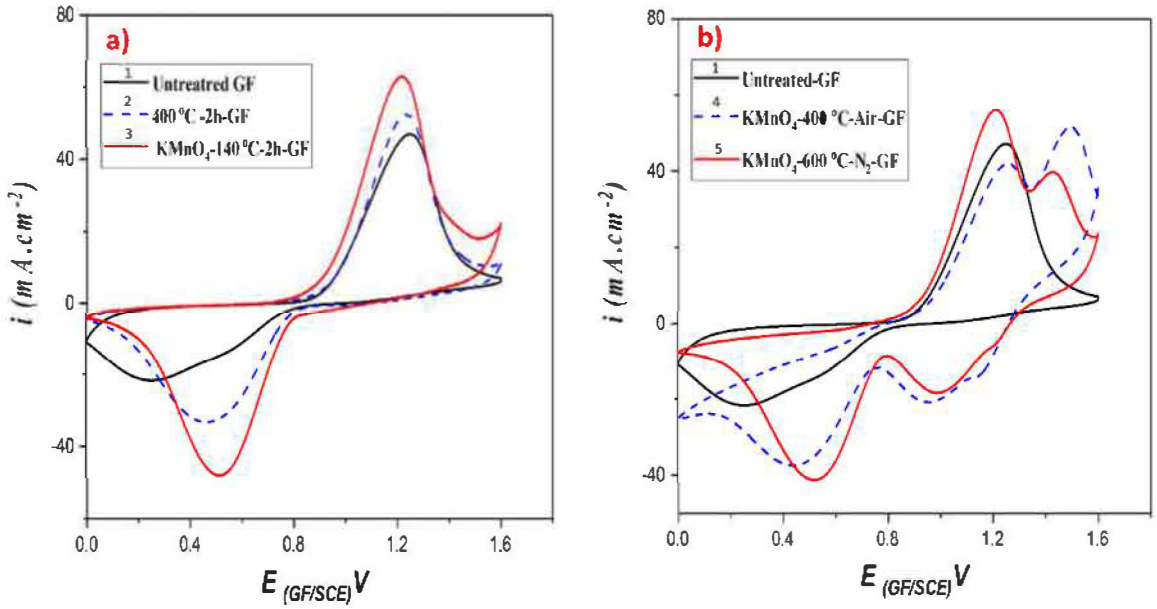

Fig. 2. a) The CV of the class-1 and b) class −2 electrodes; in 0.05 M VO^{2+} + 2 M H_2SO_4 ; at scan rate of 10 mV s^{-1}, with precisely cut 1 cm^2 of GF as working electrode, 3 cm^2 platinum foil as counter electrode and saturated calomel electrode (SCE) as reference electrode.

and treated GF was grinded to prepare samples for the FTIR analysis. 2.5 mg of the grinded powder was mixed with the 250 mg of KBr and subjected to the 10 ton of pressure to form a disk of 13 mm diameter. The modification of surface morphology and roughness of the electrode was analyzed at the acceleration voltage of the 10 KV, by the scanning electron microscopy (SEM) on the Phenom XL (Thermo Fisher scientific, USA).

3.3. Half-cell and full stack evaluation

The H-shaped divided lab scale reactor (shown in the inset of Fig. 8), was used to perform the charge discharge cycles. Initially positive half-cell was constituted by 0.5 M VO^{2+} + 3 M H_2SO_4, while the negative half-cell contained the 3 M H_2SO_4. The GF (2.25 cm^2) and platinum foil (3 cm^2) were used as the positive and negative electrodes, respectively. The saturated calomel electrode (SCE), placed in a lugging capillary, was introduced to follow the potential of the positive electrode. The full battery scale charge–discharge cycles of VRFBs were performed in filter press reactor, having 100 cm^2 of GF electrode in positive and negative electrolytic section, as shown in Fig. 1. Two storage tanks containing the anolyte and catholyte, each having the capacity of 1 L, were coupled to the electrochemical plug flow reactor. The constant flow of electrolyte was maintained through the reactor during charge and discharge process. To avoid the re-oxidation of V^{2+} by oxygen, the supply of Argon was continuously provided in the negative storage tank. The individual components of the electrochemical

reactor are shown in Fig. 1,b. As current collector, the grid of platinized titanium is inserted into the part of the GF that is outside of the electrolytic section.

4. Results and discussion

4.1. Cyclic voltammetry analysis

The CV curves were plotted to evaluate the improvement in the electrode after activations, in the 0.05 M VO^{2+} + 2 M H_2SO_4 electrolyte; between the potential ratio of 0 V to 1.6 V, at the scan rate of 10 mV s^{-1}. The scan started in the anodic direction from the open circuit potential (OCP) until 1.6 V, then it revered back towards cathodic direction until 0 V, as shown in Fig. 2.

In the analysis of the CV curves, the following performance parameters are compared; 1- anodic peak current (*Ia*), 2- cathodic peak current (*Ic*) 3- anodic to cathodic peak current ratio (*Ia / Ic*), 4- difference between the anodic and cathodic peak potentials ($\Delta E_{a/c} = E_a - E_c$). The individual peak currents correspond to the available surface area for the reactions, so any increment of the current observed, could be linked to the increase of available surface area of the electrode. The reversibility of the reactions on the electrode improves with the decrease of I_a / I_c and $\Delta E_{a/c}$, and vice versa [39].

Fig. 2,a shows the comparison of the voltammograms of the class −1 treated electrodes i-e untreated-GF, 400 °C –2h-GF and $KMnO_4$-140 °C-2 h-GF. The peak observed around 1.1 V- 1.3 V shows the oxidation of the VO^{2+} to VO_2^+, while peak in the reverse scan shows the reduction of the VO_2^+ to VO^{2+}. In the case of untreated electrode, the reverse scan does not have the well-defined peak, indicating the poor reversibility of the electrode. All the performance parameters (*Ia, Ic, Ia/Ic,* $\Delta E_{a/c}$) are improved due to the prescribed activation procedure, as summarized in the table 1. The increment of ~ 35% is observed in the magnitude of peak currents and peak potential difference is minimized by 300 mV. The improvement of the electrochemical activity of the GF is due to the oxygenal functional groups and roughness, that is fabricated on surface because of the chemical treatment. The oxygenal groups act as the catalytic sites for the VO^{2+}/VO_2^+ redox reaction. The surface roughness increases the available surface area for positive half-cell reaction and reflected in the increase of the anodic (I_a) and cathodic (I_c) currents.

Fig. 2,b shows the voltammograms of the class-2 treaded electrodes, in which the $KMnO_4$ particle are adsorbed on the electrode surface. Four peaks are observed in the CV, two in anodic directions and two in cathodic section. Peaks at 1.1 V/1.4 V and 0.4 V/0.6 V are the signals of the oxidations of VO^{2+} and reduction of VO_2^+, respectively. The additional peaks at 0.8 V/1.3 V and 1.5 V/1.6 V is due to the reduction and oxidation of $KMnO_4$ derived species, respectively. Following conclusions could be drawn from these CV observations of class-2 electrodes; 1) The residual $KMnO_4$ and all the compounds resulting from its reduction are strongly adsorbed on the surface, as the 10th cycle of the CV has the huge signal of their reduction and oxidation 2) The residual $KMnO_4$ does not exhibit any catalytic behavior against the VO^{2+}/VO_2^+ redox couple; and in addition to that, these particles are getting additional power to oxidize and reduce back on the surface. 3) There is still little increase in the peak current of VO^{2+}/VO_2^+ reaction in comparison with the untreated electrode, certainly because of the increase in the surface area of the GF .

So, the CV analysis concluded that the class-1 GF electrode, chemically activated by an acidic $KMnO_4$ solution ($KMnO_4$- 140 °C-2 h-GF) exhibits enhanced electrocatalytic activity against VO^{2+}/VO_2^+ redox reaction. On the other end, the class-2 GF electrodes having residual $KMnO_4$ particles (and derived adducts) on their surfaces, do not show any improvement against positive half- cell reaction, and will not be discussed further in the text, except in the SEM images section.

Table 1
Comparative results of the performance parameters of class- 1 electrodes. The results are extracted from Fig. 2,a voltammograms.

GF samples	I_a (mA)	I_c (mA)	I_a / I_c	$\Delta E_{a/c} = E_a - E_c$ (V)
Untreated-GF	46.9	21.7	2.16	0.99
400 °C –2h-GF	52.5	33.25	1.57	0.77
$KMnO_4$-140 °C-2 h-GF	63.1	48.03	1.31	0.70

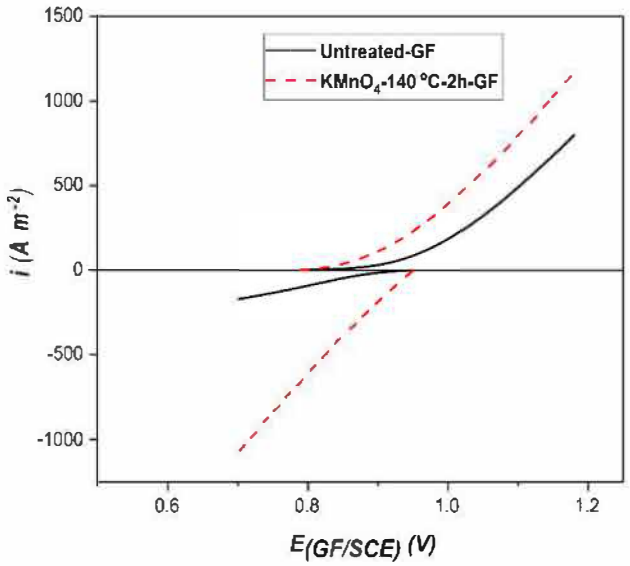

Fig. 3. LSV curves of the untreated-GF and $KMnO_4$-140 °C-2 h-GF with 2.25 cm^2 geometrical area; at r = 1 mV s^{-1}, with stirring rate 350 rpm; counter electrode = Pt 3 cm^2; Reference electrode = SCE; anolyte initial solution: 0.5 M VO^{2+} + 3 M H_2SO_4; catholyte initial solution = 0.47 < $VO^{+}_{2(M)}$ < 0.49 + 3 M H_2SO_4.

4.2. Linear sweep voltammetry (LSV) for k^o calculations

Linear sweep voltammetry was used to investigate the electro-kinetic parameters of $VO^{2+} \rightleftharpoons VO_2^+$ reaction on 'untreated-GF' and '$KMnO_4$-140 °C-2 h-GF', as shown in Fig. 3. A fresh solution containing 0.5 M VO^{2+} + 3 M H_2SO_4 was used to plot the anodic curves, while the solution obtained after electrooxidation of initial solution, was used to register the cathodic curves. The curves clearly show that the kinetics of the VO^{2+}/VO_2^+ reaction is improved by the activation procedure. The electronic transfer limited region of LSV curve ($0.7 < E_{\oplus inV/SCE} < 1.17$) is considered for the calculations of the kinetic parameters (k^o, α and β), by using simple form of the Butler Volmer Law (Eq. (3)) and the results are summarized in the table 2. The k^o value of the anodic reaction increases almost three folds (1.7 → 4.14 μm s^{-1}), while for the cathodic reaction, this enhancement is 6 times (0.9 → 5.6 μm s^{-1}).

$$I = nFSk^{\circ}C_{bulk}exp\frac{(+\alpha \ or \ -\beta)n'F}{RT}\eta \quad (3)$$

Where: η = the overvoltage; n = electron exchange number;

Table 2
Comparative data of kinetic parameters concerning redox system VO^{2+}/VO_2^+ on untreated-GF and $KMnO_4$-140 °C-2 h-GF, calculated by logarithmic analysis of the LSV curves in Fig. 3.

GF electrodes	Reaction involved	α	β	k° (μm s^{-1})
Untreated-GF	$VO^{2+} \rightarrow VO_2^+$	0.1	–	1.7
$KMnO_4$-140 °C-2 h-GF		0.17	–	4.14
Untreated-GF	$VO_2^+ \rightarrow VO^{2+}$	–	0.1	0.92
$KMnO_4$-140 °C-2 h-GF		–	0.13	5.63

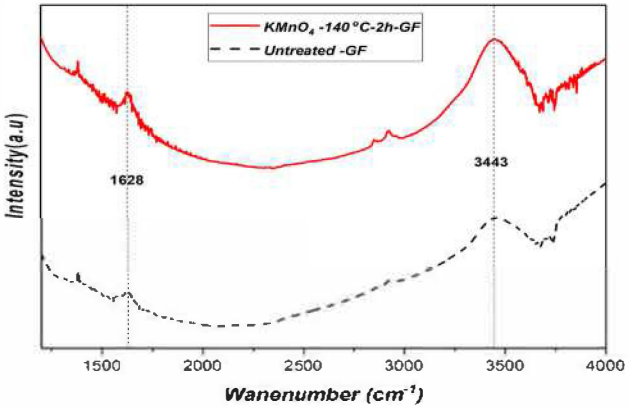

Fig. 4. FTIR spectra of the untreated-GF and the $KMnO_4$-140 °C-2 h-GF.

F = faradic constant; S = surface area; k^o = intrinsic heterogeneous electronic transfer constant; α *and* β = anodic and cathodic electronic transfer coefficients, respectively.

4.3. FTIR and SEM analysis

The surface of the electrode was characterized by FTIR analysis, before and after treatment. The obtained spectra is compared in Fig. 4. The peak at the 3443 cm^{-1} corresponds to the stretching vibration of –OH group [40], while the peak at the 1628 cm^{-1} is assigned to the hydroxyl group in enol -C = C-OH [41]. The intensity of both peaks increased after activation of the GF, thus indicating the increase in the concentration of oxygenal groups on the surface of electrode. These groups are supposed to act as catalytic sites towards the positive half-cell reaction, as the $VO^{2+} \rightleftharpoons VO_2^+$ reaction involves the oxygen transfer; and presence of the oxygen groups on the GF could possibly assist this transfer.

The changes occurred in the surface morphology of the GF were also characterized by the SEM analysis. Fig. 5 show the comparative images of *Untreated-GF* (a,b,c) and *$KMnO_4$-140 °C-2 h-GF* (d,e,f), at different magnifications. Activation method did not cause any physical damage in the overall fibrous structure, as no fragments of broken fibers are visible in Fig. 5, d. The surface of

the untreated GF is relatively smooth with some scratches; these scratches becomes sharper after activation. The sharp scratches and higher roughness provide more available surface area for the positive half-cell reactions. This observation is also consistent with the CV results, in which peak current enhanced on the *$KMnO_4$-140 °C-2 h-GF* and it is directly linked with increase of active surface area.

The SEM images of the class-2 treated electrode is shown in Fig. 6 (a,b,c). It is evident that $KMnO_4$ particles are successfully adsorbed on the GF surface. It was discussed with detail in the cyclic voltammetry section 4.1, that these particles are practically not contributing towards the vanadium reactions.

4.4. Surface free energy quantification of electrode

The better electrode–electrolyte interaction is one of the important parameters towards the kinetics of the redox reactions. The surface of the graphite felt is intrinsically hydrophobic and requires activation for the improvement of its wettability. The proposed chemical activation successfully enhanced the wettability of the electrode. To observe this electrode–electrolyte interaction, 5 µL droplet of the 0.5 M VO^{2+} + 3 M H_2SO_4 was placed on untreated-GF and $KMnO_4$-140 °C-2 h-GF. The droplet retained on the surface of the untreated GF, while it penetrates immediately in the 3D fibrous structure of treated GF, as shown in Fig. 7 a, d. This observation clearly indicates, that the activation successfully increases the surface energy of the electrode that resulted into the improvement of its wettability.

Improvement in the wettability can be quantified by surface energy calculations. For this, the semi quantitative approach is used, mentioned somewhere else [42]. Eq. (4) and (5) are representative equations for these calculations. The electrode–electrolyte contact angles of two different liquids of known dispersive and polar components are required. The $\gamma_{GF}^{P\,0.5}$ (slope) and $\gamma_{GF}^{D\,0.5}$(intercept) are obtained by the plot of $(\gamma_L(1 + cos\theta))/(2(\gamma_L^D)^{0.5})$ vs $(\gamma_L^P/\gamma_L^D)^{0.5}$.

$$\gamma_{GF} = \gamma_{GF}^P + \gamma_{GF}^D \tag{4}$$

$$\gamma_L(1 + cos\theta)/(2(\gamma_L^D)^{0.5}) = (\gamma_{GF}^P\gamma_L^P/\gamma_L^D)^{0.5} + (\gamma_{GF}^D)^{0.5} \tag{5}$$

where; γ_{GF}, γ_{GF}^P γ_{GF}^D represents the total, polar and dispersive surface free energy of electrode, respectively; And γ_L, γ_L^P , γ_L^D, indicates the total, polar and dispersive surface free energy of liquid. θ represents the electrode–electrolyte contact angle.

In this study, water and glycerol were used for the quantification of the surface energy of the GF. The untreated and treated GF was crushed and spread over the hydrophobic tape. After, the contact angles of the glycerol and water droplets (10 µL each) were precisely measured on this approximate flat surface. The contact angle of the water droplet decreased from 98.5° to 44.9° (Fig. 7 b,e), while the glycerol angle was changed from 93.5° to 34.3° (Fig. 7 c,f). The results of the surface free

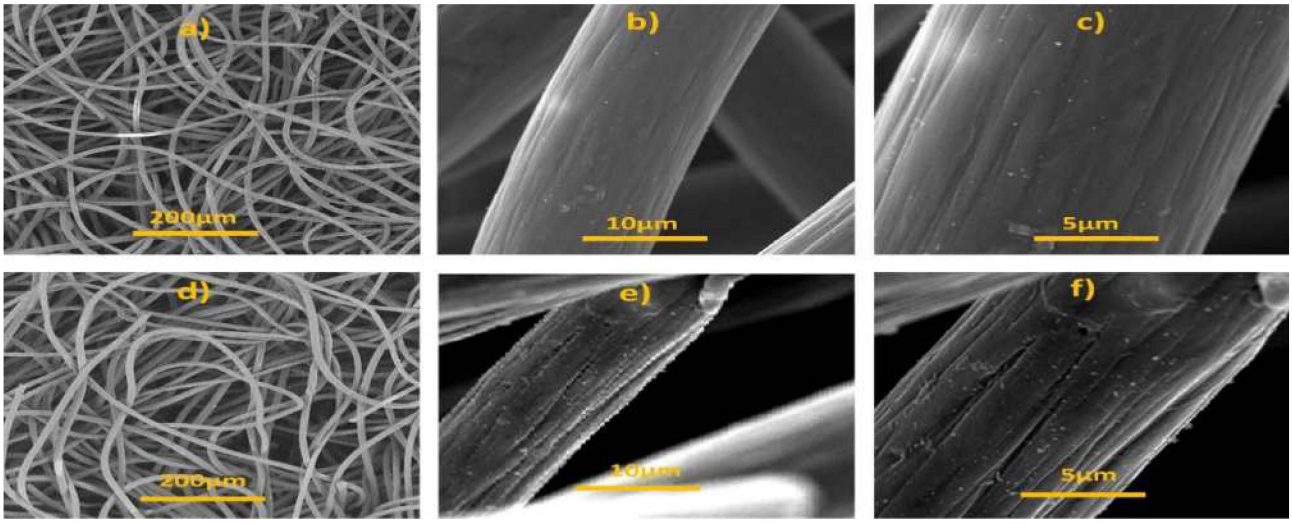

Fig. 5. The surface morphology characterization of the untreated GF (a,b,c) and $KMnO_4$-140 °C-2 h-GF (d,e,f), at different magnifications.

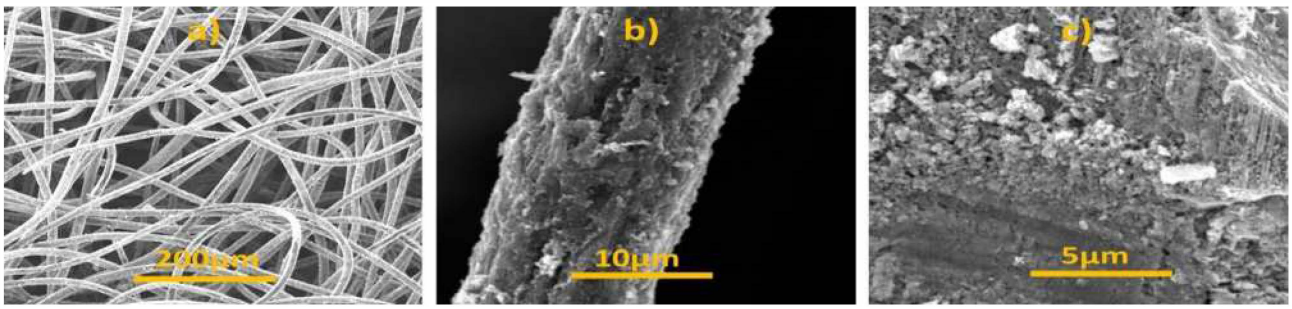

Fig. 6. SEM images of the $KMnO_4$-600 °C-N_2-GF at different magnifications (class 2 electrode).

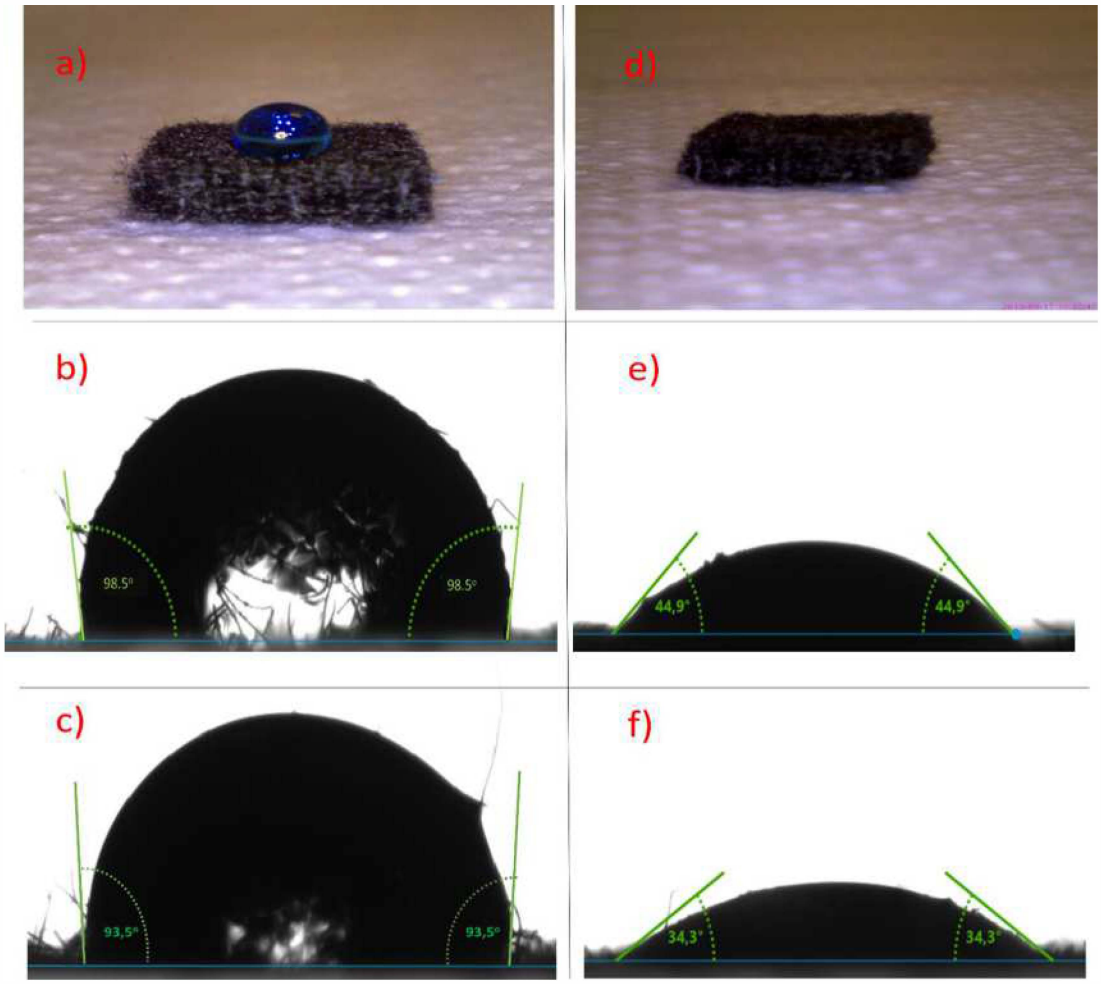

Fig 7. Wettability evaluation by placing 5 µL droplet of 0.5 M VO^{2+} + 3 M H_2SO_4 on untreated GF(a) and $KMnO_4$-140 °C-2 h-GF(d); The 10 µL droplet of water on untreated GF (b) and $KMnO_4$-140 °C-2 h-GF (e); 10 µL droplet of glycerol on untreated GF (c) and $KMnO_4$-140 °C-2 h-GF (f).

energy calculations are summarized in table 3

Due to activation of electrode, the surface free energy is increased from 13.9 mN/m to 53.29 mN/m. This increment is responsible for the better wettability and electrode–electrolyte interaction.

4.5. Charge-Discharge cycles

To evaluate the performance of activated GF against $VO^{2+} \rightleftarrows VO_2^+$ reaction, charge–discharge cycles were performed in following two different reactors, 1) *H shaped divided electrochemical cell* and 2) *filter press divided electrochemical reactor.* The electrolysis was carried out under galvanostatic conditions at constant current density.

4.5.1. H shaped divided electrochemical cell

The electrolysis was initially performed in H type divided cell, as shown in the inset of Fig. 8. The posolyte was constituted by 0.5 M VO^{2+} + 3 M H_2SO_4 , while the negolyte was an aqueous solution of 3 M sulfuric acid. Operating in a half-cell enables to check the performance of the positive electrode without having any interference from the reactions involved at the negative electrode. The posolyte was mechanically stirred at 350 rpm, while the stirring conditions in negolyte was indigenously established by the H_2 bubbles, produced during protons electro-reduction.

The electrolysis was performed in anodic direction at constant current density of 667 A m^{-2}, enabling the oxidation of $V^{(IV)}$ to $V^{(V)}$. The electrolysis was carried out until the working electrode voltage

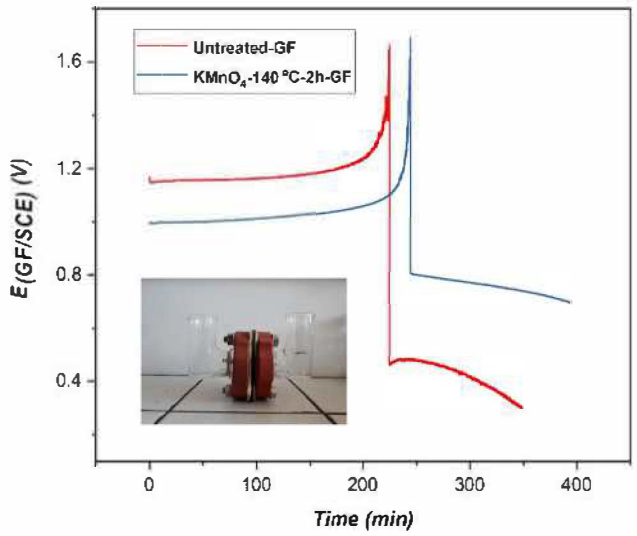

Fig. 8. Evolution of the working electrode potential of untreated-GF and $KMnO_4$-140 °C-2 h-GF, during charge- discharge electrolysis, performed in a H shaped divided electrochemical cell (inset). Nafion membrane is used for separation of electrolytic compartments. posolyte: 0.5 M VO^{2+} + 3 M H_2SO_4; negolyte: 3 M H_2SO_4; S_{GF}: 2.25 cm^2

Table 3
The results of surface free energy calculations of untreated GF and $KMnO_4$-140 °C-2 h-GF.

Electrode	γ_{GF}^{P}(mN/m)	γ_{GF}^{D} = (mN/m)	γ_{GF}(mN/m)
Untreated GF	6.5	7.4	13.9
$KMnO_4$-140 °C-2 h-GF	30.25	23.04	53.29

approached 1.65 V. Then the cathodic current density of 667A m^{-2} was applied to convert back $V^{(V)}$ to $V^{(IV)}$. The voltage evolution of charge–discharge electrolysis of *untreated-GF* and *$KMnO_4$-140 °C-2 h-GF* is shown in Fig. 8. Due to the activation of GF, the average charging voltage decreased from 1.18 V to 1.04 V and average discharge voltage increased from 0.42 V to 0.75 V. These observations confirm the positive effect of the treatment on the electrode, as the decrease of the overvoltage translates to the increase in energy and voltage efficiency. Three consecutive charge–discharge cycles were performed to check the durability of electrode performance; and the electrode maintained the performance during these cycles.

4.5.2. Filter press divided electrochemical reactor

The *filter press electrochemical reactor* was used to perform the charge–discharge cycles under galvanostatic mode, to evaluate the performance of electrode on the full-scale redox flow battery. Both, posolyte and the negolyte were initially constituted by 0.5 M VO^{2+} + 3 M H_2SO_4. The initial volume of the posolyte (500 ml) was double than the negolyte to compensate the difference in the electrolysis duration, induced by the electron's ratio ($V^{IV} \rightarrow VO^{V}$)/($V^{IV} \rightarrow V^{II}$) = 1/2. The electrolysis was carried out under a constant current of 0.5 A (S_{GF} = 100 cm^2), until the cell voltage reached 2 V; then the applied current decreased to 0.35 A, and the electrolysis pursued again until the cell voltage approached 2 V. This sequence was repeated in two additional stages at 0.2 A and 0.1 A respectively, until the 80% state of charge (SOC) of battery was achieved. After it, half volume of the posolyte was removed, and subsequently charge–discharge cycle was performed under galvanostatic conditions by using *untreated-GF* and *$KMnO_4$-140 °C-2 h-GF* electrodes. The constant current density of 50 A m^{-2} was applied during charge discharge cycles. 2 V was set as the upper voltage limit, because the solvent tends to oxidize at higher voltages and can be observable in the form of O_2 evolution. On the other end, the release of H_2 is also possible in the negative electrode compartment if the applied current is higher than the total limiting current of the successive reduction of VO^{2+} to V^{2+}.

The cell voltage evolution during electrolysis for electrolyte preparation, is shown in the Fig. 9, a. Only the first and last voltage point is plotted at each current. The cell voltage is lower in the case of treated electrode than the untreated electrode, during all the operation. The observation indicates the enhanced electrocatalytic behavior of the activated electrode.

Cell voltage curves during charge–discharge cycle are shown in Fig. 9, b. Due to activation of electrode, the average charging voltage decreased from 1.86 V (untreated) to 1.76 V (treated) and average discharging voltage increased from 0.59 V (untreated) to 0.80 V (treated) . At a current density of 50 A m^{-2}, there is an improvement of 20% and 13% in energy and voltage efficiency (VE), respectively. This observation reveals that, in comparison with untreated electrode, the

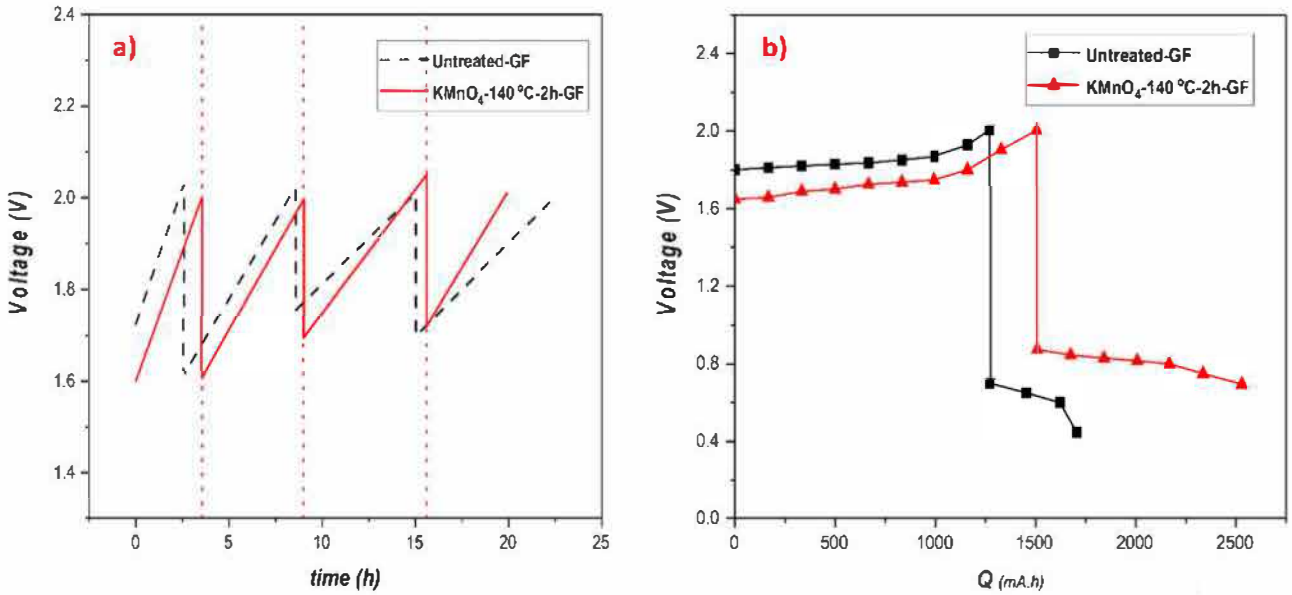

Fig. 9. a) cell evolution during the electrolyte preparation by using untreated GF and $KMnO_4$-140 °C-2 h-GF; b) charge discharge cycles of untreated GF and $KMnO_4$-140 °C-2 h-GF in the stack with positive and negative electrode of geometrical area of 100 cm^2.

activated electrode requires lower power for charging; and obtained power during discharge is higher. Also, the duration of the charging and discharging is prolonged, resulted in the higher conversions.

5. Conclusion

The proposed chemical method successfully activated the GF, to be used as positive electrode in the VRFBs. In the CV analysis , ~35% enhancement was observed in the peak current of $VO^{2+} \rightleftharpoons VO_2^+$ redox reaction. The electronic transfer kinetic constant (k^o) of charge and discharge reactions in positive half-cell, were enhanced by 2.6 and 6.1 times, respectively. The surface free energy calculations by contact angle measurements reveals that the electrode–electrolyte affinity was improved after activation that plays an important role in the surface catalysis. The surface oxygenal groups, integrated during activation process was expectedly catalyzing the positive half-cell reactions. Moreover, the available surface area for the reactions was enhanced because the activation made the surface rough and grooved. The activated GF showed the promising results during charge–discharge cycles, conducted at the following two different reactors 1) *H-shaped divided electrochemical cell* and 2) *filter press divided electrochemical reactor*. The prescribed activation process is operationally very easy, as it does not require any complicated procedures .

6. Financials

This work was supported by ANR (L'Agence nationale de la recherche, France) and the Campus France.

CRediT authorship contribution statement

Ali Hassan: Conceptualization, Methodology, Investigation, Writing - original draft, Formal analysis, Validation. **Theodore Tzedakis:** Conceptualization, Methodology, Supervision, Writing - review & editing, Validation.

Declaration of Competing Interest

The authors declare that they have no known competing financial interests or personal relationships that could have appeared to influence the work reported in this paper.

Acknowledgments

The authors would like to acknowledge Ms. Brigitte Dustou for providing technical support regarding the filter press divided electrochemical reactor. We are also very grateful to Dr. Fabien Chauvet for his technical support for the contact angle measurements.

References

[1] A.Z. Weber, M.M. Mench, J.P. Meyers, P.N. Ross, J.T. Gostick, Q. Liu, Redox flow batteries: A review, J. Appl. Electrochem. 41 (2011) 1137–1164, https://doi.org/10.1007/s10800-011-0348-2.

[2] Y.K. Zeng, T.S. Zhao, L. An, X.L. Zhou, L. Wei, A comparative study of all-vanadium and iron-chromium redox flow batteries for large-scale energy storage, J. Power Sources. 300 (2015) 438–443, https://doi.org/10.1016/j.jpowsour.2015.09.100.

[3] H. Zhou, H. Zhang, P. Zhao, B. Yi, A comparative study of carbon felt and activated carbon based electrodes for sodium polysulfide/bromine redox flow battery, Electrochim. Acta. 51 (2006) 6304–6312, https://doi.org/10.1016/j.electacta.2006.03.106.

[4] H. Vafiadis, M. Skyllas-Kazacos, Evaluation of membranes for the novel vanadium bromine redox flow cell, J. Memb. Sci. 279 (2006) 394–402, https://doi.org/10.1016/j.memsci.2005.12.028.

[5] D.J. Park, K.S. Jeon, C.H. Ryu, G.J. Hwang, Performance of the all-vanadium redox flow battery stack, J. Ind. Eng. Chem. 45 (2017) 387–390, https://doi.org/10.1016/j.jiec.2016.10.007.

[6] L. Cao, A. Kronander, A. Tang, D.W. Wang, M. Skyllas-Kazacos, Membrane permeability rates of vanadium ions and their effects on temperature variation in vanadium redox batteries, Energies. 9 (2016), https://doi.org/10.3390/en9121058.

[7] C. Choi, S. Kim, R. Kim, Y. Choi, S. Kim, H. young Jung, J.H. Yang, H.T. Kim, A review of vanadium electrolytes for vanadium redox flow batteries, Renew. Sustain. Energy Rev. 69 (2017) 263–274. doi:10.1016/j.rser.2016.11.188.

[8] M. Skyllas-Kazacos, L. Cao, M. Kazacos, N. Kausar, A. Mousa, Vanadium Electrolyte Studies for the Vanadium Redox Battery—A Review, ChemSusChem. 9 (2016) 1521–1543, https://doi.org/10.1002/cssc.201600102.

[9] L. Joerissen, J. Garche, C. Fabjan, G. Tomazic, Possible use of vanadium redox-flow batteries for energy storage in small grids and stand-alone photovoltaic systems, J. Power Sources. 127 (2004) 98–104, https://doi.org/10.1016/j.jpowsour.2003.09.066.

[10] M. Skyllas-Kazacos, All-Wanadium Redox Battery, United States Pat. (1988).

[11] M. Zhang, M. Moore, J.S. Watson, T.A. Zawodzinski, R.M. Counce, Capital Cost Sensitivity Analysis of an All-Vanadium Redox-Flow Battery, J. Electrochem. Soc. 159 (2012) A1183–A1188, https://doi.org/10.1149/2.041208jes.

[12] A. Di Blasi, O. Di Blasi, N. Briguglio, A.S. Aricò, D. Sebastián, M.J. Lázaro, G. Monforte, V. Antonucci, Investigation of several graphite-based electrodes for vanadium redox flow cell, J. Power Sources. 227 (2013) 15–23, https://doi.org/10.1016/j.jpowsour.2012.10.098.

[13] C. Flox, J. Rubio-Garcia, R. Nafria, R. Zamani, M. Skoumal, T. Andreu, J. Arbiol, A. Cabot, J.R. Morante, Active nano-CuPt3 electrocatalyst supported on graphene for enhancing reactions at the cathode in all-vanadium redox flow batteries, Carbon N. Y. 50 (2012) 2372–2374, https://doi.org/10.1016/j.carbon.2012.01.060.

[14] A. Bourke, M.A. Miller, R.P. Lynch, X. Gao, J. Landon, J.S. Wainright, R.F. Savinell, D.N. Buckley, Electrode Kinetics of Vanadium Flow Batteries: Contrasting Responses of V^{II}-V^{III} and V^{IV}-V^{V} to Electrochemical Pretreatment of Carbon, J. Electrochem. Soc. 163 (2016) A5097–A5105, https://doi.org/10.1149/2.0131601jes.

[15] R. Schweiss, T. Oelsner, F. Dörfler, A. Davydov, S. Wöhner, A. Hirschvogel, Recent Insights into Carbon Felt Electrodes for Redox, Flow Batteries (2011).

[16] K.J. Kim, S.W. Lee, T. Yim, J.G. Kim, J.W. Choi, J.H. Kim, M.S. Park, Y.J. Kim, A new strategy for integrating abundant oxygen functional groups into carbon felt electrode for vanadium redox flow batteries, Sci. Rep. 4 (2014) 1–6, https://doi.org/10.1038/srep06906.

[17] A. Hassan, T. Tzedakis, Enhancement of the electrochemical activity of a commercial graphite felt for vanadium redox flow battery (VRFB), by chemical treatment with acidic solution of K2Cr2O7, J. Energy Storage. 26 (2019) 100967, , https://doi.org/10.1016/j.est.2019.100967.

[18] P. Mazúr, J. Mrlík, J. Beneš, J. Pocedič, J. Vrána, J. Dundálek, J. Kosek, Performance evaluation of thermally treated graphite felt electrodes for vanadium redox flow battery and their four-point single cell characterization, J. Power Sources. 380 (2018) 105–114, https://doi.org/10.1016/j.jpowsour.2018.01.079.

[19] T. Liu, X. Li, C. Xu, H. Zhang, Activated Carbon Fiber Paper Based Electrodes with High Electrocatalytic Activity for Vanadium Flow Batteries with Improved Power Density, ACS Appl. Mater. Interfaces. 9 (2017) 4626–4633, https://doi.org/10.1021/acsami.6b14478.

[20] Z. He, Y. Jiang, H. Zhou, G. Cheng, W. Meng, L. Wang, L. Dai, Graphite felt electrode modified by square wave potential pulse for vanadium redox flow battery, Int. J. Energy Res. 41 (2017) 439–447, https://doi.org/10.1002/er.3626.

[21] Y.C. Chang, J.Y. Chen, D.M. Kabtamu, G.Y. Lin, N.Y. Hsu, Y.S. Chou, H.J. Wei, C.H. Wang, High efficiency of CO2-activated graphite felt as electrode for vanadium redox flow battery application, J. Power Sources. 364 (2017) 1–8, https://doi.org/10.1016/j.jpowsour.2017.07.103.

[22] J. Kim, H. Lim, J.Y. Jyoung, E.S. Lee, J.S. Yi, D. Lee, Effects of Doping Methods and Kinetic Relevance of N and O Atomic Co-Functionalization on Carbon Electrode for V(IV)/V(V) Redox Reactions in Vanadium Redox Flow Battery, Electrochim. Acta. 245 (2017) 724–733, https://doi.org/10.1016/j.electacta.2017.06.008.

[23] Z. He, Y. Jiang, W. Meng, F. Jiang, H. Zhou, Y. Li, J. Zhu, L. Wang, L. Dai, HF/H2O2treated graphite felt as the positive electrode for vanadium redox flow battery, Appl. Surf. Sci. 423 (2017) 111–118, https://doi.org/10.1016/j.apsusc.2017.06.154.

[24] J. Kim, H. Lim, J.Y. Jyoung, E.S. Lee, J.S. Yi, D. Lee, High electrocatalytic performance of N and O atomic co-functionalized carbon electrodes for vanadium redox flow battery, Carbon N. Y. 111 (2017) 592–601, https://doi.org/10.1016/j.carbon.2016.10.043.

[25] D.M. Kabtamu, J.Y. Chen, Y.C. Chang, C.H. Wang, Water-activated graphite felt as a high-performance electrode for vanadium redox flow batteries, J. Power Sources. 341 (2017) 270–279, https://doi.org/10.1016/j.jpowsour.2016.12.004.

[26] X.L. Zhou, Y.K. Zeng, X.B. Zhu, L. Wei, T.S. Zhao, A high-performance dual-scale porous electrode for vanadium redox flow batteries, J. Power Sources. 325 (2016) 329–336, https://doi.org/10.1016/j.jpowsour.2016.06.048.

[27] B. Sun, M. Skyllas-Kazakos, Chemical modification and electrochemical behaviour of graphite fibre in acidic vanadium solution, Electrochim. Acta. 36 (1991) 513–517, https://doi.org/10.1016/0013-4686(91)85135-T.

[28] H. Zhou, Y. Shen, J. Xi, X. Qiu, L. Chen, ZrO2-Nanoparticle-Modified Graphite Felt: Bifunctional Effects on Vanadium Flow Batteries, ACS Appl. Mater. Interfaces. 8 (2016) 15369–15378, https://doi.org/10.1021/acsami.6b03761.

[29] B. Li, M. Gu, Z. Nie, X. Wei, C. Wang, V. Sprenkle, W. Wang, Nanorod niobium oxide as powerful catalysts for an all vanadium redox flow battery, Nano Lett. 14 (2014) 158–165, https://doi.org/10.1021/nl403674a.

[30] H. Zhou, J. Xi, Z. Li, Z. Zhang, L. Yu, L. Liu, X. Qiu, L. Chen, CeO2 decorated graphite felt as a high-performance electrode for vanadium redox flow batteries, RSC Adv. 4 (2014) 61912–61918, https://doi.org/10.1039/c4ra12339e.

[31] X. Wu, H. Xu, L. Lu, H. Zhao, J. Fu, Y. Shen, P. Xu, Y. Dong, PbO2-modified graphite felt as the positive electrode for an all-vanadium redox flow battery, J. Power Sources. 250 (2014) 274–278, https://doi.org/10.1016/j.jpowsour.2013.11.021.

[32] A.A. Shah, H. Al-Fetlawi, F.C. Walsh, Dynamic modelling of hydrogen evolution

effects in the all-vanadium redox flow battery, Electrochim. Acta. 55 (2010) 1125–1139, https://doi.org/10.1016/j.electacta.2009.10.022.
[33] H. Al-Fetlawi, A.A. Shah, F.C. Walsh, Modelling the effects of oxygen evolution in the all-vanadium redox flow battery, Electrochim. Acta. 55 (2010) 3192–3205, https://doi.org/10.1016/j.electacta.2009.12.085.
[34] M.H. Chakrabarti, R.A.W. Dryfe, E.P.L. Roberts, Evaluation of electrolytes for redox flow battery applications, Electrochim. Acta. 52 (2007) 2189–2195, https://doi.org/10.1016/j.electacta.2006.08.052.
[35] M. Gattrell, J. Park, B. MacDougall, J. Apte, S. McCarthy, C.W. Wu, Study of the Mechanism of the Vanadium 4+/5+ Redox Reaction in Acidic Solutions, J. Electrochem. Soc. 151 (2004) A123, https://doi.org/10.1149/1.1630594.
[36] K.J. Kim, M.-S. Park, Y.-J. Kim, J.H. Kim, S.X. Dou, M. Skyllas-Kazacos, A technology review of electrodes and reaction mechanisms in vanadium redox flow batteries, J. Mater. Chem. A. 3 (2015) 16913–16933, https://doi.org/10.1039/C5TA02613J.
[37] I. Bureau, Wo 2016/164017, (2016).
[38] Y. Jiang, X. Feng, G. Cheng, Y. Li, C. Li, Z. He, J. Zhu, W. Meng, H. Zhou, L. Dai, L. Wang, Electrocatalytic activity of MnO2 nanosheet array-decorated carbon paper as superior negative electrode for vanadium redox flow batteries, Electrochim. Acta. 322 (2019) 134754, , https://doi.org/10.1016/j.electacta.2019.134754.
[39] Z. González, C. Flox, C. Blanco, M. Granda, J.R. Morante, R. Menéndez, R. Santamaría, Outstanding electrochemical performance of a graphene-modified graphite felt for vanadium redox flow battery application, J. Power Sources. 338 (2017) 155–162, https://doi.org/10.1016/j.jpowsour.2016.10.069.
[40] X. Wu, H. Xu, P. Xu, Y. Shen, L. Lu, J. Shi, J. Fu, H. Zhao, Microwave-treated graphite felt as the positive electrode for all-vanadium redox flow battery, J. Power Sources. 263 (2014) 104–109, https://doi.org/10.1016/j.jpowsour.2014.04.035.
[41] C. Gao, N. Wang, S. Peng, S. Liu, Y. Lei, X. Liang, S. Zeng, H. Zi, Influence of Fenton's reagent treatment on electrochemical properties of graphite felt for all vanadium redox flow battery, Electrochim. Acta. 88 (2013) 193–202, https://doi.org/10.1016/j.electacta.2012.10.021.
[42] V.G. Papadakis, Estimation of Estimation of, J. Appl. Polym. Sci. 13 (1969) 1741–1747.